Low-Latitude Pi2 Waves according to Observations on *SWARM* Satellites and Ground Stations

V. A. Martines-Bedenko[a], V. A. Pilipenko[b, *], E. N. Fedorov[a], E. Nahayo[c], and E. Yizengaw[d]

[a]*Schmidt Institute of Physics of the Earth, Russian Academy of Sciences, Moscow, 123995 Russia*
[b]*Geophysical Center, Russian Academy of Sciences, Moscow, 119296 Russia*
[c]*South African National Space Agency, Pretoria, Gauteng, 0087 South Africa*
[d]*Boston College, Boston, Massachusetts, USA*
***e-mail: pilipenko_va@mail.ru**
Received March 31, 2018; revised June 12, 2018; accepted September 20, 2018

Abstract—We considered wave disturbances of the Pi2 type geomagnetic field (periods of 1–2 min) recorded simultaneously by magnetometers at low-latitude stations in Africa and on low-orbit *SWARM* satellites both during the beginning of a substorm and in non-substorm periods. At night, Pi2 waves in the upper ionosphere and on Earth are almost identical in amplitude and in phase. These waves on the satellite mainly manifest themselves in longitudinal (along the geomagnetic field) and radial magnetic components. A comparison of the observational results with the model of the interaction of MHD waves with the ionosphere—atmosphere—Earth system shows that night low-latitude Pi2 signals are generated by magnetospheric fast magnetosonic waves propagating to the Earth through the opacity region. The results of analytical estimates and numerical simulations are consistent with the properties of Pi2 signals recorded in the upper ionosphere and on Earth.

1. INTRODUCTION: MECHANISMS OF DISTRIBUTION TRANSMISSION OF Pi2 TYPE DISTURBANCES TO LOW LATITUDES

The damping quasi-periodic Pi2 pulse is traditionally considered an indicator of explosive energy release during the beginning onset of a substorm. Pi2 signals also accompany many pulsed and dynamic processes in the tail of the magnetosphere [8]. Most clear Pi2 signals are visible at mid and low latitudes, because high-latitude Pi2 pulsations, apparently, have a different physical nature and are strongly masked by intense geomagnetic variations at the beginning of substorm activation [12]. Existing ideas relate the periodic response at low latitudes to dynamic phenomena in the night magnetosphere with resonant excitation of volume cavity magnetosonic vibrations oscillations in the plasmasphere or virtual plasmasphere resonance [7, 20]. The concept of Pi2 as the vibrational oscillatory magnetohydrodynamic (MHD) response of the internal magnetosphere to dynamic processes in the geomagnetic tail was confirmed by satellite observations in the night magnetosphere [17]. These oscillations were recorded as periodic variations in the oblateness of the magnetospheric magnetic field, usually identified with fast magnetosonic (FMS) waves. These ideas are supported by theoretical modeling based on the consideration of magnetosonic oscillations of the plasma volume enclosed between two boundaries: the ionosphere and plasmapause [10].

The possibility of detecting ultra-low-frequency (ULF) waves in the upper ionosphere on low-orbit satellites has significantly supplemented the physics of the interaction of MHD waves with the ionosphere [4, 13], since until recently the existing concepts were mainly based on either ground-based or magnetospheric observations. Using observations on the *CHAMP* satellite, it was for the first time possible to single out Pi2 pulsations in vector magnetometer data in the upper ionosphere [16]. These observations showed the predominance of parallel (compression component) magnetic field B_P in the polarization structure of Pi2 pulsations at low altitudes (~500 km). The B_P component of night Pi2 waves on the satellite coincided well in amplitude and phase with the X (N-S) component of these waves on Earth. Pi2 disturbances recorded by the *Orsted* satellite (~640–840 km) at low latitudes also predominantly represented oblateness waves of the geomagnetic field [6]. Magnetsonic waves of the Pi2 type and the ground response to them were recorded at night on the *CHAMP* satellite and at low-latitude stations [5].

The satellite observations listed above were interpreted based on the ideas that night Pi2 oscillations at low latitudes are caused by magnetosonic volume cavity plasmasphere oscillations penetrating Earth's sur-
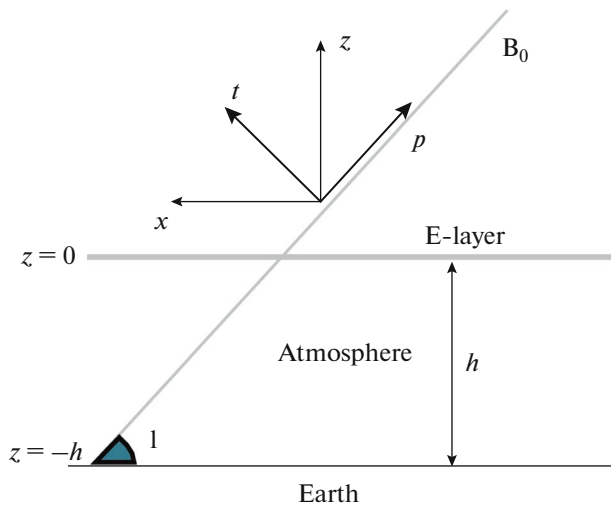
Fig. 1. Coordinate systems used in the paper: in the $\{x, y, z\}$ system, the axes are directed to the equator, east and up, respectively, the $\{t, y, p\}$ coordinate system is oriented along geomagnetic field $\mathbf{B}_0$.

face. Although this qualitative interpretation of satellite and ground-based observations of Pi2 pulsations in previous papers is not in doubt, no quantitative comparisons with theoretical models of the interaction of MHD waves with the ionosphere were carried out. Consideration of synchronously recorded Pi2 pulsations at low-latitude magnetic stations and on low-orbit satellites yielded paradoxical at first sight results: in the field of a magnetosonic wave, the parallel B_P component (along the geomagnetic field) turned out to be of the same order of magnitude as the transverse B_T component (perpendicular to the geomagnetic field) [16].

In this paper, we consider the structure of Pi2 type oscillations synchronously recorded on a pair of low-orbit *SWARM-A* and *SWARM-C* satellites and on the ground-based low-latitude magnetometer network in Africa. The results are compared with the predictions of a numerical model of the interaction of magneto-

spheric MHD waves with the multilayer ionosphere–atmosphere–Earth system.

2. SATELLITE AND GROUND-BASED MAGNETOMETERS

Three identical probes, *SWARM-A*, -*B*, and -*C*, were launched in November 2013 into an almost circular near-polar (inclination of 87.3°) orbit in the following configuration: spacecraft *A* and *C* move side by side ~1.1° apart in longitude at an altitude of 460 km; spacecraft *B* moves in its independent orbit at an altitude of 530 km. The *SWARM* satellites were equipped with a wide range of highly sensitive new-generation instruments: vector magnetometer, absolute scalar magnetometer, Langmuir probe for measuring density, plasma drift, and electric field, and GPS receiver.

During analysis, the data of the three-component magnetometer were transformed into coordinate system $\{t, y, p\}$ with the p axis directed along the current geomagnetic field $\mathbf{B}_0$. The field components in this orthogonal coordinate system shown in Fig. 1 are the parallel B_P, transverse radial B_T, and transverse azimuthal B_y components.

To monitor the ground response to ULF waves, the 1-s data from the AMBER magnetometer network in Africa (http://magnetometers.bc.edu) was used, and then supplemented by the data from the INTERMA-GNET station network (http://www.intermagnet.org), and the Hermanus station of the South African Space Agency (https://www.sansa.org.za). Codes and the geographical and geomagnetic coordinates (latitude Φ and longitude Λ) of stations are given in Table 1. The data of ground-based magnetometers are presented in the $\{x, y, z\}$ coordinate system with components of field $\mathbf{B} = \{X, Y, Z\}$ (Fig. 1). In this Cartesian system, the x, y, z axes are directed to south, east, and up, respectively (Fig. 1).

We looked at *SWARM-A* and -*C* passages over Africa at night in 2015 searching distinct quasi-periodic disturbances in the Pi2 range (30 s to 2 min). Events were selected, where Pi2 pulsations were

Table 1. Magnetic stations in Africa

Stations	Code	Geographic latitude	Geographic longitude	Geomagnetic latitude	Geomagnetic longitude	Network
Medea	ALGR	36.85	02.93	28.0	77.7	AMBER
Yaounde	CMRN	03.87	11.52	−05.3	83.1	AMBER
Conakry	CNKY	10.50	−13.70	−00.5	60.4	AMBER
Abuja	ABJA	10.50	07.55	0.6	79.6	AMBER
Addis Ababa	AAE	09.03	38.77	7.1	111.6	INTERMAGNET
Tamanrasset	TAM	22.79	05.53	11.6	79.0	INTERMAGNET
Hermanus	HER	−34.43	19.23	−42.3	84.1	SANSA

Geomagnetic coordinates are calculated using the data from https://omniweb.gsfc.nasa.gov/vitmo/.

recorded on the satellite at low latitudes and at a small distance from the geomagnetic equator. In the data of both ground-based and satellite magnetometers, the low-frequency trend is removed using a high-frequency filter with a cutoff period of 120 s.

3. EXAMPLES OF TYPICAL Pi2 EVENTS

From the simultaneous signals of the Pi2 type recorded in 2015 at night on satellites and on Earth, we present typical examples. At low latitudes, Pi2 pulsations are manifested at ground stations mainly in the X-component (N-S) [15], therefore, the data of only this component are presented. The maps of satellite passages show the vertical projections of the orbits of spacecraft A and C, the position of the geomagnetic (dip) equator, and the recording stations.

October 15, 2015 (Day 288)

At 22:10−22:20 UT, the satellites flew along the eastern coast of Africa around midnight (LT ~ 0.6) (Fig. 2a). The satellites passed over the geomagnetic equator around 22:13 UT.

A coherent Pi2 signal was observed at all stations at geomagnetic latitudes from 0° to ~40° (Fig. 2b). The largest oscillation amplitude on satellites was observed in the parallel and transverse components: $B_P \sim 2.5$ nT and $B_T \sim 1.2$ nT. In the azimuthal component, the disturbance is weaker $B_y \sim 0.8$ nT. On Earth under a satellite (the AAE station), the amplitude of the Pi2 pulse $X \sim 2$ nT is slightly less than on the satellite.

The appearance of Pi2 pulsations corresponded to the beginning of the growth of the auroral AE index, which indicates that this pulse is caused by the beginning onset of a substorm.

January 3, 2015 (Day 003)

At 1:25−01:38 UT, the satellites' orbit passed through central Africa (LT ~ 2.2) (Fig. 3a). Above the geomagnetic equator, the satellites passed around 22:31 UT.

On Earth, a global irregular disturbance of the Pi2 type was observed (Fig. 3b). The amplitude of the Pi2 signal at the station under the satellite (CMRN) reached $X \sim 2.5$ nT. On the satellite itself, the field disturbance was somewhat smaller, $B_P \sim 2$ nT and $B_T \sim 1.6$ nT. The disturbance in the B_y component is weaker and did not correlate with the other components.

The signal was recorded at the time of the beginning of the growth of the AE index, which indicates its excitation at the beginning onset of the substorm.

At the HER station ($\Phi \sim -42°$), the field variations are found to be in antiphase with the equatorial CMRN and CNKY stations. This can indicate that the HER and near-equatorial stations are located on different sides of the intrinsic oscillation node of the plasmasphere [20].

January 17, 2015 (Day 017)

At 23:20−23:40 UT (LT ~ 0.9), when the satellites flew in the region of central Africa, the Pi2 pulse was synchronously recorded at all ground stations (Fig. 4a). Above the geomagnetic equator, satellites passed at about 22.32 UT.

Although the satellite data on the magnetic field were noisy in this event, we can single out weak Pi2 pulsations, whose amplitude at the beginning of the pulse was $B_P \sim 0.7$ nT, $B_T \sim B_y < 0.4$ nT (Fig. 4b). At the CMRN station located at approximately the same geomagnetic latitude as the satellites, the disturbance amplitude was somewhat larger than $X \sim 1.2$ nT.

The Pi2 pulse was observed against a relatively quiet background ($AE < 80$ nT), therefore it is not caused by the beginning onset of a substorm. This event is an example of Pi2 pulsations not associated with the substorm activation [9].

4. MODEL OF FMS WAVE DISTRIBUTION THROUGH THE IONOSPHERE TO EARTH

Like previous observations on the *CHAMP* and *Orsted* satellites, the *SWARM* data showed that the FMS mode makes the main contribution to the structure of Pi2 waves in the upper ionosphere at low latitudes. This mode is identified by the presence of the parallel magnetic component B_P (the magnetic field oblateness component). Therefore, a quite adequate model for describing Pi2 pulsations in the upper ionosphere can be the consideration of the interaction of the FMS wave with the multilayer magnetosphere−ionosphere−atmosphere−the Earth system. For waves with periods $T > 10$ s, the thickness of the conductive E-layer is less than the skin length of the MHD wave, and this layer can be approximated by an anisotropic conductive film at an altitude h above the Earth with Pedersen and Hall integral height-integrated conductivities Σ_P and Σ_H. Above the E-layer there is the magnetosphere, which we will represent as a half-space filled with cold plasma and immersed in the uniform direct straight magnetic field $\mathbf{B}_0$ inclined at the angle I to the ionospheric layers. Magnetic inclination $I > 0$ in the northern and $I < 0$ in the southern hemispheres and vertical $\mathbf{B}_0$ correspond to $I = \pm \pi/2$. The magnetospheric plasma is characterized by Alfvén velocity V_A and wave conductivity $\Sigma_A = 1/\mu_0 V_A$. The thin E-layer is at $z = 0$, and Earth's surface is at $z = -h$. It is assumed that the atmosphere is an isotropic dielectric with complex permittivity $\varepsilon_a = \varepsilon_0 + i\sigma_a$, and the Earth is an isotropic conductor with conductivity σ_g. In the horizontal direction, i.e., along x and y, the system is homogeneous.

Our consideration is based on the results of the theory of the thin ionosphere [3]. The wave electric ($\mathbf{E}$)
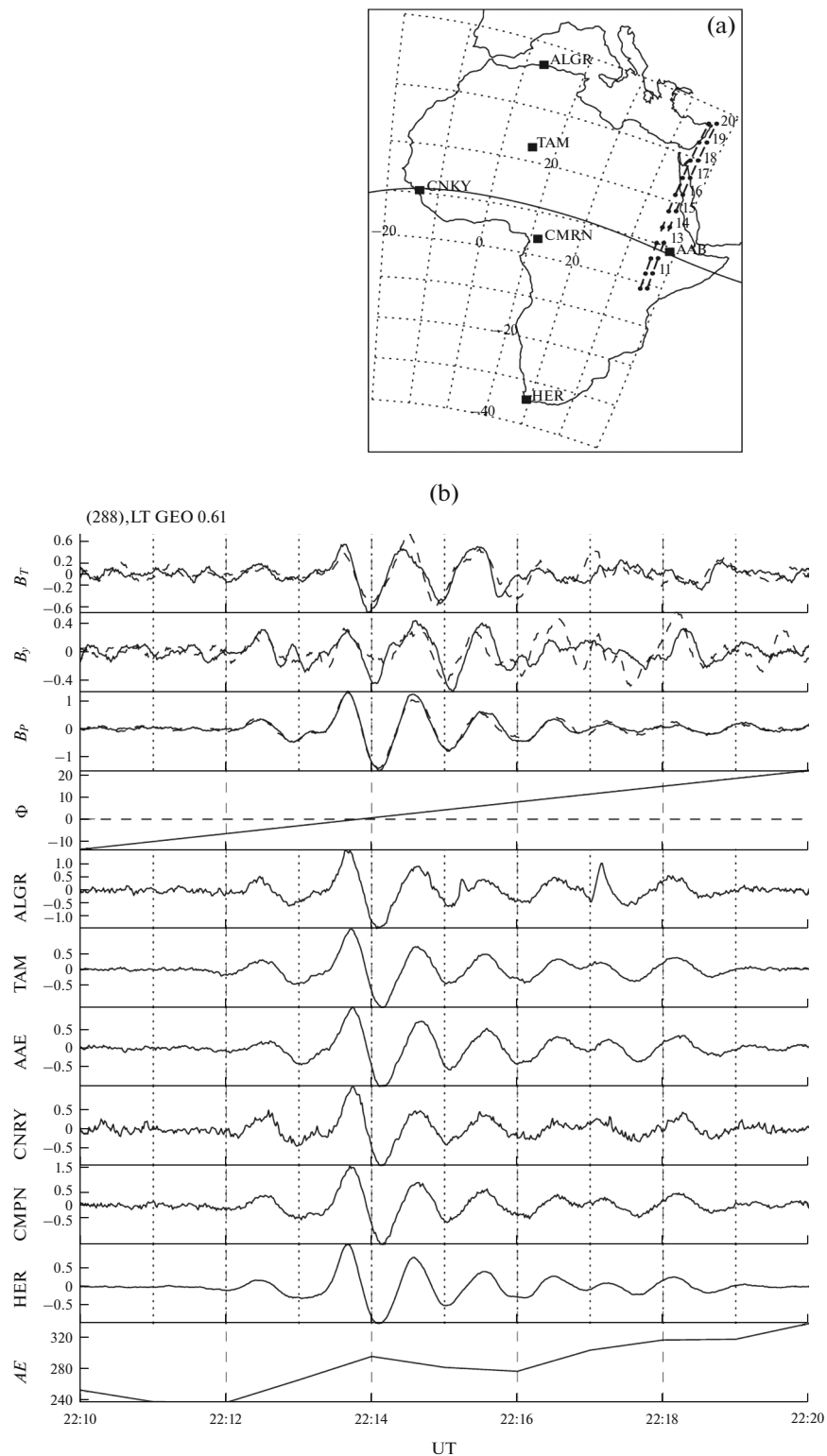
Fig. 2. Low-latitude Pi2 oscillations recorded by stations in Africa and the *SWARM-A* and *-C* satellites on October 15, 2015. Top, map with the vertical projection of the orbits and the positions of the magnetic stations. The dashed lines show the grid of geomagnetic coordinates, the line is the geomagnetic (dip) equator. Local time of the passage is given in the GSE coordinate system. Bottom, the magnetic B_T, B_y, and B_P components on the satellites (solid lines for A and dashed for C), geomagnetic latitudes of the satellites Φ, X is the component of the pulsations at ground stations, and AE index.
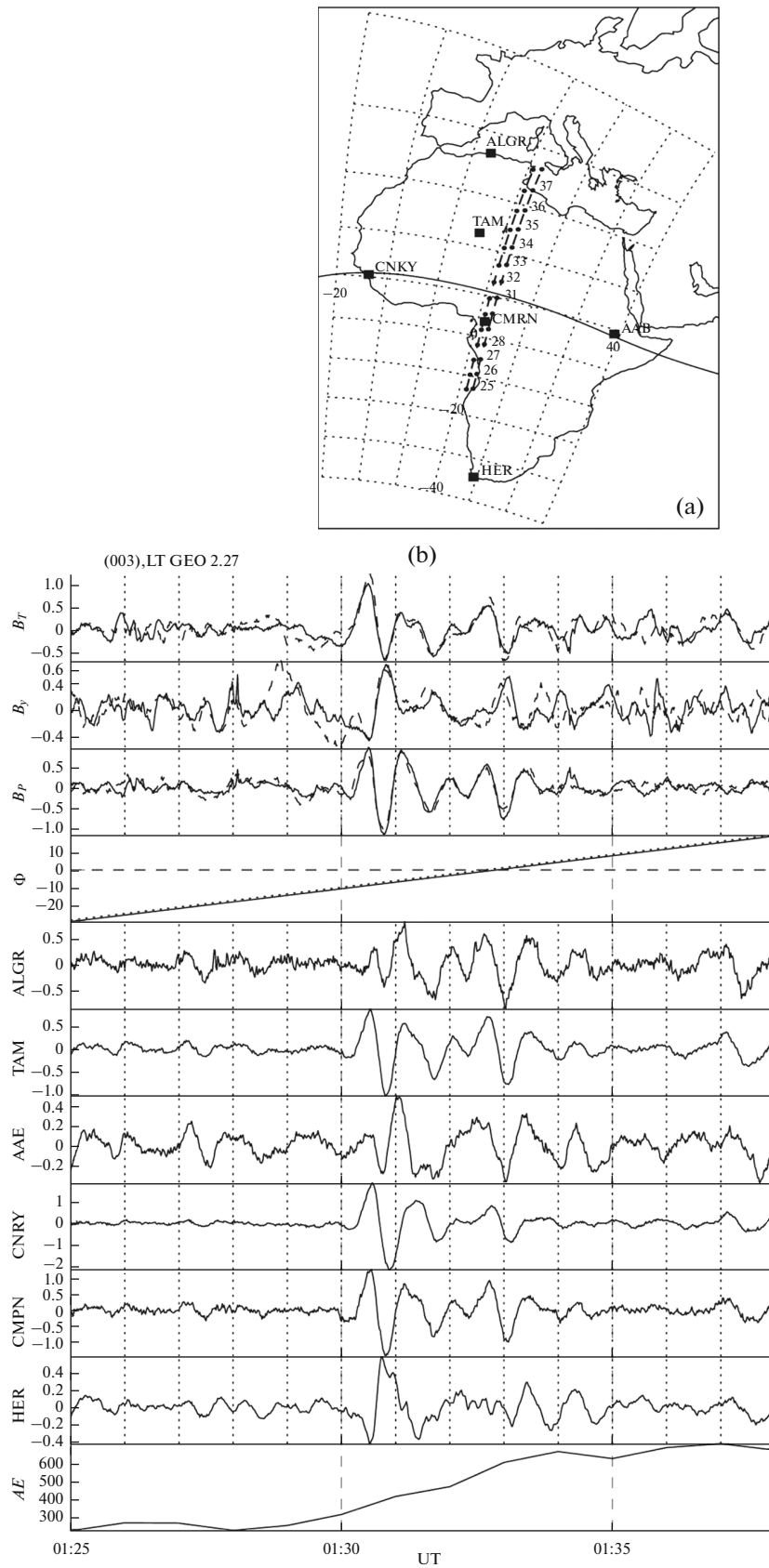
Fig. 3. Data from the satellite and ground-based magnetometers for January 3, 2015 (in the same format as in Fig. 2): top, map with the projection of the orbits and the position of the magnetic stations; bottom, the magnetic B_T, B_y, and B_P components on the *SWARM* satellites, geomagnetic latitude of the satellites Φ, *X*-component of pulsations at ground stations, and *AE* index.
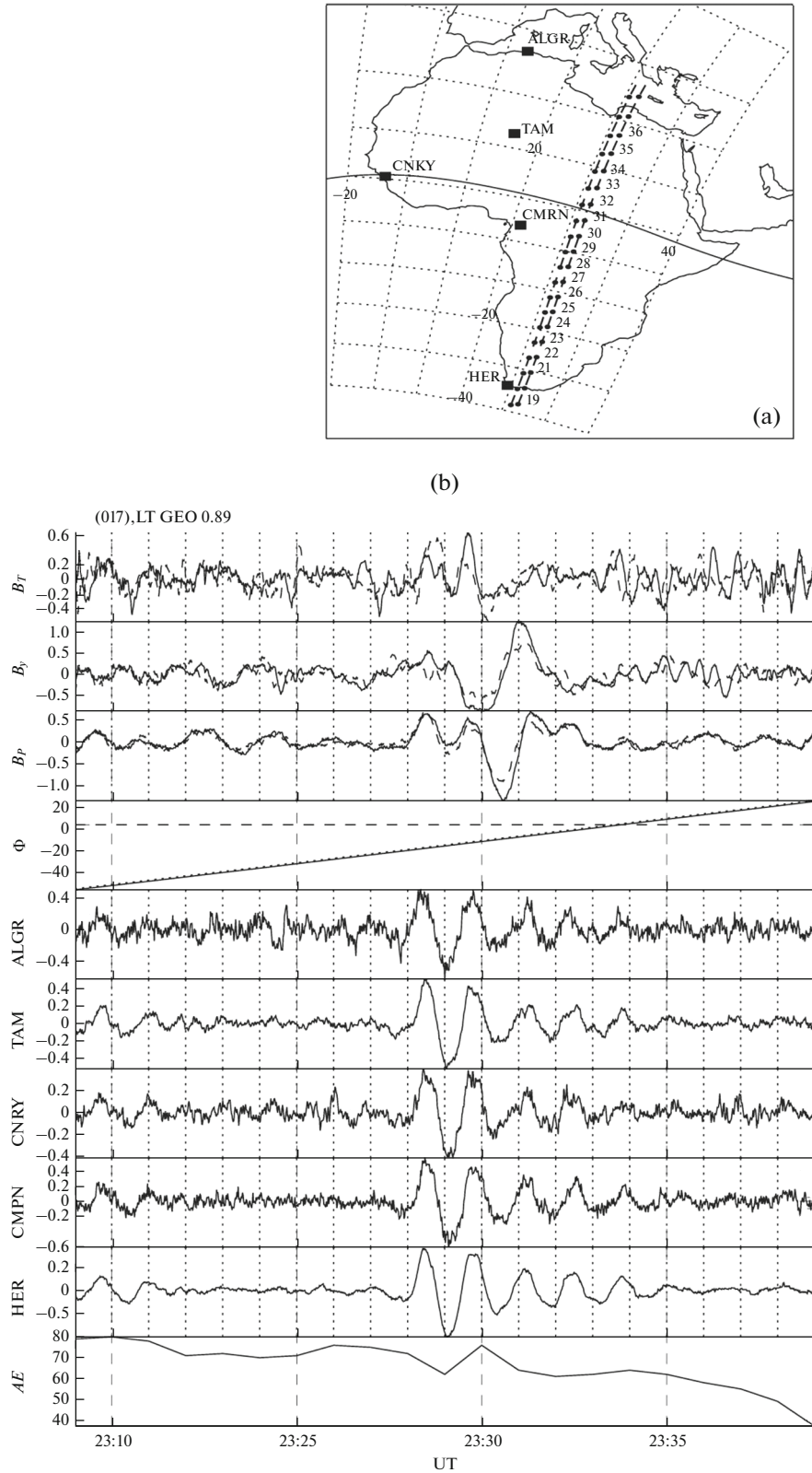
Fig. 4. Synchronous data of the satellite and ground-based magnetometers for January 17, 2015 (in the same format as in Fig. 2): top, map with the projection of the orbits and the position of the magnetic stations; bottom, the magnetic B_T, B_y, and B_P components on the *SWARM* satellites, geomagnetic latitude of the satellites Φ, X-component of pulsations at ground stations, and *AE* index.

and magnetic (**B**) fields can be decomposed into two modes. Magnetospheric fields are the sum of:

—Alfvén mode (A), in which the disturbed magnetic field $B_\perp$ is perpendicular to B_0, and the parallel magnetic component $B_P = 0$;

—magnetosonic mode (F), in which the transverse magnetic field $B_\perp$ is the vortex-free and parallel component of the electric current $j_P = 0$.

In turn, the electromagnetic disturbance in the atmosphere consists of:

—magnetic H-mode, in which the vertical component of the disturbed electric field is absent $E_z = 0$, and

—electric E-mode, in which the vertical component of the disturbed magnetic field $Z = 0$.

The polarization of the magnetospheric Alfvén mode corresponds to the polarization of the electric mode in the atmosphere, and the polarization of the magnetosonic mode corresponds to the polarization of the H mode in the atmosphere. The general system of Maxwell equations and linearized quasi-hydrodynamic equations in magnetospheric-ionospheric plasma is split into two coupled systems for the A and F modes. In the atmosphere, equations for the E and H modes are disengaged.

The electromagnetic field in the magnetosphere above the E-layer can be represented as a combination of incident and reflected waves. For theoretical estimates, we consider the harmonic of the incident wave $\exp(-i\omega t + ik_x x + ik_y y)$, where ω is the wave frequency, $\mathbf{k}_\perp = \{k_x, k_y\}$ is the horizontal wave number. Since only large-scale magnetospheric modes with small k_y can reach the ionosphere, we neglect the azimuthal variations of the wave field, i.e., we set $k_y = 0$. This assumption is consistent with the absence of a time shift between the Pi2 signals on spacecraft A and C separated in the longitude by ~1°. Then, magnetospheric MHD modes have the following properties:

—The incident Alfvén wave has azimuthal magnetic component B_y, while the transverse radial component $B_T = 0$ and the parallel (along B_0) component $B_P = 0$.

—The falling FMS mode has the nonzero parallel B_P component. In this case, transverse radial component B_T is generally not equal to zero.

The propagation of the FMS mode deep into the magnetosphere substantially depends on the relation between horizontal component **k** of the wave vector and Alfvén wave number $k_A = \omega/V_A$. When the FMS wave is incident on the ionosphere with relatively large transverse wave numbers, so that $k^2 > k_A^2$ (i.e., with scales $1/k < 10^5$ km in the Pi2 range), the wave, when propagating, falls into the inner plasmasphere into the opacity region, where the square of the radial component of the wave vector is negative, $k_x^2 < 0$. However,

due to the large scales, even the decaying FMS mode can reach Earth's surface.

For the FMS mode in the opacity region (a typical situation for waves of the Pi2 range in the upper ionosphere and plasmasphere) above the E-layer of the ionosphere, the ratio of the total parallel and radial components has form

$$\frac{B_P}{B_T} = \frac{\cos I - ikh_* \sin I}{\sin I + ikh_* \cos I}. \tag{1}$$

This formula describes the relation between the total amplitudes of the incident wave and the wave reflected from the Earth with finite conductivity. Here, $h_* = h + (1 + i)\delta_g/2$ is the effective altitude of the ionosphere for the finite Earth's conductivity, $\delta_g = \sqrt{2/\omega\mu_0\sigma_g}$ is the skin-length for Earth with conductivity σ_g. With the infinite conductivity of Earth $h_* \to h$. Far from the geomagnetic equator ($I \neq 0$), the parallel and transverse components should be commensurate with each other.

At equatorial latitudes ($I \to 0$), where $B_P \to B_x$ and $B_T \to B_z$, relation (1) gives

$$\frac{B_z}{B_x} = -ikh_*. \tag{2}$$

From (2) it follows that above the highly conductive Earth for $kh \ll 1$, $k\delta_g \ll 1$, the amplitude of the vertical magnetic component of the FMS wave in the upper ionosphere should be much less than the horizontal, $|B_z| \ll |B_x|$.

When passing through the ionosphere, the ellipse of magnetosonic wave polarization does not rotate, i.e., the dominant horizontal component both on Earth and in the ionosphere are the X-components. The latitudinal distribution of the amplitude of the FMS wave in the magnetosphere is determined by its diffraction on a sphere with dense plasma (internal plasmasphere). By analogy with the similar problem for the diffraction of electromagnetic wave on a conducting ball [1], it can be assumed that the disturbance of the resulting structure should decrease with latitude Φ with distance from the equatorial plane as $B_P \propto \cos\Phi$. This circumstance, at least in part, explains the decrease in the amplitude of the Pi2 waves observed in the upper ionosphere, when the satellite moves away from the geomagnetic equator [6].

The efficiency of the passage of the FMS wave through the ionosphere to Earth's surface can be characterized by the ratio between the total amplitudes (the sum of the incident and reflected waves) of horizontal component B_x of the disturbance above the E-layer of the ionosphere and ground response $B_x^{(g)}$. Combining relations from [3], we obtain

$$\frac{B_x}{B_x^{(g)}} = \frac{1 - ip + kh_*}{1 + kh_*} e^{kh}, \tag{3}$$

where $p = \omega h_*/V_C$, $V_C = (\mu_0\Sigma_C)^{-1}$ are the "Cowling" velocity determined by the Cowling ionospheric conductivity $\Sigma_C = \Sigma_P + \Sigma_H^2/\Sigma_P$ (for approximate estimates, the relation V_C [km/s] $\approx 800/\Sigma_C$ [S] can be used). Relation (3) shows that waves with small compared to the altitude of the ionosphere scales $kh > 1$ weakly penetrate to Earth's surface. The passage of large-scale ($kh < 1$) FMS modes through the ionosphere to Earth is controlled by parameter p. If $|p| \ll 1$, the ionosphere can be considered transparent for the FMS mode, and the incident wave is mainly reflected from Earth's surface. If $|p| \sim 1$, then the ionosphere partially shields the magnetospheric signal from ground-based magnetometers, and only when $|p| \gg 1$, the FMS mode is mainly reflected from the ionosphere.

We use coefficient κ_F from [14], which characterizes the ratio of the total amplitude of the parallel wave component in the ionosphere at altitude z to the magnetic disturbance on Earth's surface. At small altitudes relative to the E-layer of the ionosphere, where $kz \ll 1$, $\cos kz \approx 1$, and $\sin kz/k \approx z$, the expression for κ_F reduces to the following

$$k_F(z) = \frac{B_P(z)}{B_x^{(g)}} = -\frac{1-ip}{1+kh}[\cos I - ik(h_* + z)\sin I]. \quad (4)$$

Factor κ_F depends on the latitude of the observation point. In the dipole geomagnetic field, the inclination of magnetic field I is related to geomagnetic latitude Φ as $\tan I = 2\cot\Phi$. For the large-scale mode $kz \ll 1$ for $I \ne \pi/2$ from (4), we obtain $|\kappa_F| = \cos I(1 - ip)/(1 + kh_*)|$. Relation $|\kappa_F|$ decreases with increasing the latitude as $|\kappa_F| \propto \cos I$. Also $|\kappa_F|$ grows with frequency, because h_* and $|p|$ grow with frequency. At low latitudes at night, when $|p| \ll 1$, $|kh_*| \ll 1$, the field on Earth $B_x^{(g)}$ should be slightly larger than B_P on the satellite. This circumstance is due to the fact that the FMS wave is reflected mainly from Earth, while the incident and reflected waves are added near Earth's surface.

For typical conductivities for the night ionosphere, Pi2 pulsation range, and Earth's conductivity $(\sigma_g \to \infty)$, the parameter $|p| \ll 1$, which means that the ionosphere cannot have a noticeable effect on the propagation of the FMS mode to Earth's surface. In the general case, the field of the magnetosonic mode is quite sensitive to the conductivity of the planet's surface; therefore, finite conductivity σ_g can noticeably affect the FMS field of the wave recorded on a low-orbit satellite [2].

Although in general the above theoretical estimates are in fairly good agreement with the properties of the recorded Pi2 oscillations, further we will give the results of a more rigorous numerical calculation without the simplifications made above.

5. NUMERICAL CALCULATIONS OF THE FMS WAVE PASSAGE TO EARTH'S SURFACE

Here, we present the results of a numerical calculation considering completer and more accurate, but also bulkier formulas from [3]. These relations take into account such additional effects that were neglected in simplified analytical estimates: the excitation of the surface ionospheric mode due to the Hall effect, the presence of finite conductivity of the atmosphere $(\sigma_a \ne 0)$ and Earth $(\sigma_g \ne \infty)$, and finite azimuthal wave scale $(k_y \ne 0)$. The transverse wave scale is a critical parameter, therefore, the rations between the amplitudes of the wave components will be given depending on wave number $k \equiv k_x$. The range of possible wave numbers is from $k = k_A = 8 \times 10^{-5}$ km^{-1} (when the wave becomes almost transverse to $\mathbf{B}_0$) to $k = 10^{-1}$ km^{-1}. According to ground-based observations, the characteristic scale of disturbances is on the order of magnitude of 10^3 km, which corresponds approximately to the range $k \sim 10^{-3}$–10^{-4} km^{-1}. The azimuthal component of the wave vector is assumed $k_y = 10^{-4}$ km^{-1}. The graphs show the total amplitudes (the sum of the incident and reflected modes).

The boundary condition on Earth's surface ($z = -h$) is expressed through the impedance relation for a homogeneous conducting half-space. If the skin-length in the Earth is much smaller than the transverse scale of the disturbance $k\delta_g \ll 1$, then this relation is determined by impedance $Z_g = \exp(-i\pi/4)\sqrt{\omega\mu/\sigma_g}$. Conductivities of the homogeneous atmosphere and Earth's crust $\sigma_a = 10^{-14}$ S/m, and $\sigma_g = 10^{-3}$ S/m.

The results of numerical calculation for the incident magnetosonic wave of the Pi2 range ($T = 100$ s) are presented for the following parameters: $V_A = 800$ km/s, $\Sigma_A \sim 1$ S. The ionospheric conductivities correspond to the night low-latitude ionosphere: $\Sigma_H = 0.8$ S, $\Sigma_P = 0.4$ S, the altitude of the E-layer $h = 100$ km. It is assumed that observations are carried out at the altitude of $z = 400$ km above the E-layer of the ionosphere at low geomagnetic latitudes in the northern hemisphere with the inclination of $I = 30°$. When calculating, it was assumed that in the incident FMS wave, the amplitude of the parallel component for all k is constant $B_P^{(i)}$ (400 km) $= 1$ nT.

The reflection efficiency of a magnetosonic wave from the planar ionosphere−atmosphere−Earth system is characterized by the R_{FF} reflection coefficient (Fig. 5). The numerical model confirms that the FMS wave is well reflected, $R_{FF} \sim 1$, at scales of $\sim 10^3$ km. At small scales ($1/k < 200$ km), the wave reflection sharply worsens. When magnetosonic wave is incident, a reflected Alfvén mode also arises due to mode conversion in the anisotropic E-layer, but its excitation efficiency characterized by the R_{AF} coefficient is small.
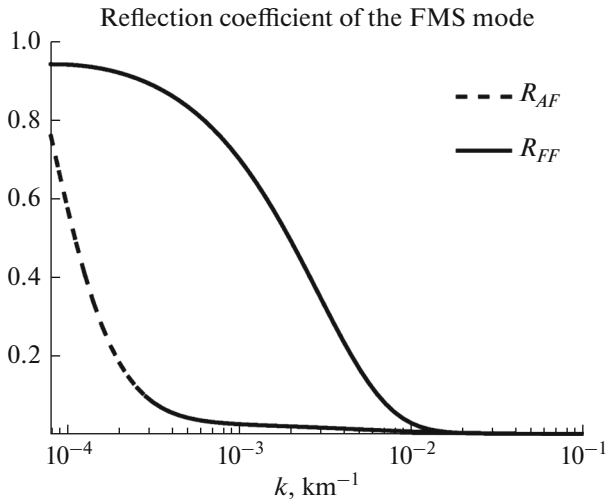
Fig. 5. Dependence on the radial component of the wave vector of the reflection coefficient of the incident magnetosonic wave $R_{FF}(k)$ and the transformation coefficient into the reflected Alfvén mode $R_{AF}(k)$.

Figure 6 shows the amplitudes of the wave components in the ionosphere at the altitude $z_* = 400$ km above Earth's surface, depending on wave number k of the incident FMS wave. For wave numbers $k > 10^{-2}$ km^{-1}, reflection coefficient R_{FF} is small (see Fig. 5), so that the reflected FMS wave can be neglected, and as a result $|B_P| \cong |B_T| \cong B_P^{(i)} = 1$ nT. When decreasing the wave number, the amplitude of transverse component B_T decreases with the formation of minimum at $k = k_A$. In the region of spatial scales characteristic for Pi2, the
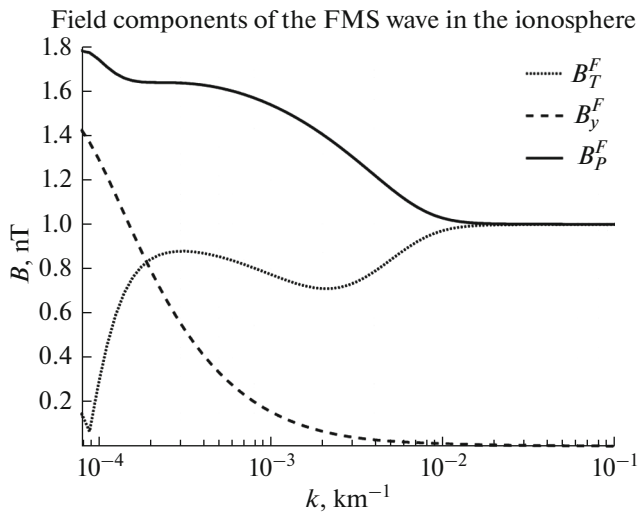
amplitude of the component $B_P \sim 1.5$ nT is approximately greater by a factor of 2 than the amplitude of the component $B_T \sim 0.8$ nT.

The parallel component B_P slowly increases with decreasing k to ~ 1.75 nT. This increase is due to the addition of the magnetic fields of the incident and reflected waves when reflecting from the well-conducting Earth and the small attenuation of the reflected wave at small k. For $k > k_y$, the B_y component is small, with decreasing k it grows and compares with the other components for $k \sim k_y$, it even exceeds B_T at $k < k_y$ (this is formally due to variation in the spatial structure of the initial wave).

Figure 7 shows the amplitude of the disturbance of the magnetic field on Earth's surface from the incident FMS wave. Waves with wave numbers $k > 10^{-2}$ km^{-1} do not reach Earth's surface due to rapid attenuation. Waves with k from 10^{-2} to 4×10^{-5} km^{-1} slightly attenuate, when passing through the ionosphere. Due to the superposition of the incident and reflected waves, the amplitude of ground response $B_x^{(g)}$ is found to be ~ 1.7 times larger than the amplitude of the parallel component of the incident wave. Component $B_y^{(g)}$ is small, and is compared to $B_x^{(g)}$ only for $k \sim k_y$.

6. DISCUSSION OF RESULTS

In the vast majority of events recorded by the *SWARM* satellites at low latitudes, Pi2 pulsations were observed in parallel B_P and transverse B_T components with comparable amplitudes, with a prevalence of B_P over B_T by a factor of 1.3–2.1. The amplitude of the

Fig. 6. Amplitudes of the magnetic components B_T, B_y, and B_P in the upper ionosphere ($z = 400$ km) during the fall of the magnetosonic mode with $B_P^{(i)} = 1$ nT and different latitudinal scales (characterized by wave number k).
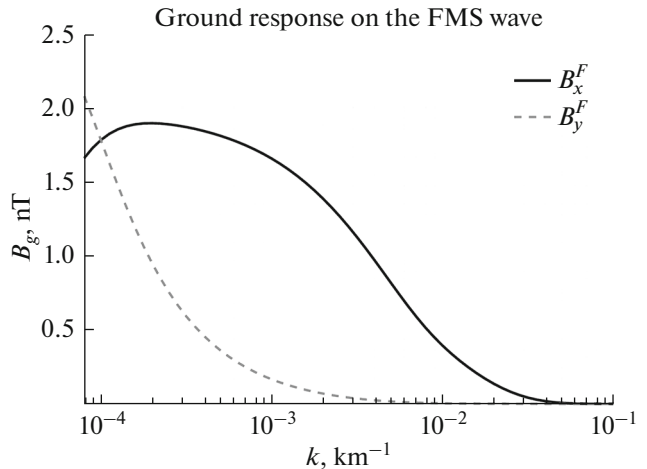

Fig. 7. Amplitude of the ground response for the $B_x^{(g)}$ and $B_y^{(g)}$ components to the incident magnetosonic wave with $B_P^{(i)} = 1$ nT and different latitudinal scales (characterized by wave number k).

X-component of the signal at the ground station (it corresponds to the theoretically calculated value $B_x^{(g)}$) near the orbit projection was slightly larger (by a factor of 1.1−1.8) than the amplitude of the parallel B_P component on the satellite. The characteristic properties of the structure of Pi2 pulsations, both excited at the time of auroral activation and those observed against a quiet background, were identical. The features of low-latitude Pi2 pulsations are well interpreted by a theoretical model based on the consideration of the incidence of the FMS wave on the plane-layered ionosphere−atmosphere−Earth system. The smallness of the B_y component on the satellite and the Y component on Earth is due to the large scale of the wave in the azimuthal direction. The relationship between B_P and B_T components is characteristic for the FMS wave in the opacity region. The same relation was observed on magnetospheric satellites in the inner magnetosphere ($L < 3.5$) [17]. The large amplitude of the signal on Earth compared with the satellite is the result of a superposition of the incident and reflected from the Earth magnetosonic waves.

The presented numerical model describes the local relation between the amplitudes of the components of the wave field specified by the spatial harmonic of the $\propto \exp(ik_x x + ik_y y)$ form. In the real magnetosphere, a standing wave is formed between conjugated ionospheres, which will lead to a variation in the phase relations between the field components. For example, in the vicinity of the equatorial plane of the magnetosphere ($s = 0$), the parallel (along the field line) field structure $B_P(s) \sim \cos(k_\parallel s)$ and $B_T(s) \sim \sin(k_\parallel s)$, thus, the B_P and B_T components must be in phase in one hemisphere and antiphase in the other.

Formally, the developed numerical model cannot be directly applied to the geomagnetic equator region, where $I \to 0$ and in a narrow band with width of ~2°−3°, the effective conductivity of the ionosphere is determined by the Cowling conductivity. However, the dimension of this region is small compared to the scale of Pi2 pulsations, and it will not noticeably affect the interaction of the magnetosonic wave with the ionosphere.

An analysis of Pi2 events recorded at mid-latitudes at a noticeable distance from the geomagnetic equator (not presented in the paper) showed that the relations between the components begin to differ from the theoretically predicted ones (1). Apparently, this is due to the fact that the assumption on the incident wave as a purely magnetosonic mode is violated, and the Alfvén component contributes to the field of Pi2 pulsations. The possibility of linking coupling the FMS wave with the Alfvén mode at mid latitudes was predicted by theoretical modeling [11, 19], and was suggested based on the radar Pi2 observations in the ionosphere [18].

In plasma measurements on *SWARM* satellites, FMS waves can manifest themselves as relative variations in density $\Delta N/N$ with the amplitude on the order of magnitude of relative variations in the magnitude of magnetic field $\Delta B/B \sim (2-6) \times 10^{-5}$. However, at near equatorial latitudes in the ionospheric plasma density measured in the satellite localized jumps often occur due to plasma bubbles. Against the background of these density jumps with the relative intensity of $\Delta N/N \sim (2-8) \times 10^{-3}$, it is difficult to single out density variations caused by Pi2 pulsations, which should have 2 orders of magnitude lower amplitude.

CONCLUSIONS

The *SWARM* satellite magnetometers are capable to reliably to detect even weak ULF signals with the amplitude of no more than several thousandths of a percent of the geomagnetic field. Consideration of synchronously recorded Pi2 pulsations at low-latitude magnetic stations and at a low-orbit *SWARM* satellite showed that in the wave field the parallel component (along the geomagnetic field) only slightly exceeds the transverse radial component in amplitude, and the amplitude of the ground response exceeds the wave amplitude in the upper ionosphere. Simple analytical estimates and more rigorous numerical simulations have shown that these properties of Pi2 signals are in good agreement with the ideas about the interaction with the ionosphere−atmosphere−Earth system of magnetospheric magnetosonic waves propagating to Earth through the opacity region in the internal plasmasphere.

REFERENCES

1. Landau, L.D. and Lifshits, E.M., *Teoreticheskaya fizika* (Theoretical Physics), vol. 8: *Elektrodinamika sploshnykh sred* (Electrodynamics of Continuous Media), Moscow: Nauka, 1987.

2. Fedorov, E.N. and Pilipenko, V.A., Electromagnetic sounding of planets from a low-orbiting probe, *Cosmic Res.*, 2014, vol. 52, no. 1, pp. 46−51.

3. Alperovich, L.S. and Fedorov, E.N., *Hydromagnetic Waves in the Magnetosphere and the Ionosphere*, Springer, 2007.

4. Balasis, G., Papadimitriou, C., Zesta, E., and Pilipenko, V., Monitoring ULF waves from low Earth orbit satellites, *Waves, Particles, and Storms in Geospace*, Oxford University Press, 2016, pp. 148−169.

5. Cuturrufo, F., Pilipenko, V., Heilig, B., Stepanova, M., Luhr, H., Vega, P., and Yoshikawa, A., Near-equatorial Pi2 and Pc3 waves observed by CHAMP and on SAMBA/MAGDAS stations, *Adv. Space Res.*, 2015, vol. 55, pp. 1180−1189.

6. Han, D.-S., Iyemori, T., Nose, M., et al., A comparative analysis of low latitude Pi2 pulsations observed by Ørsted and ground stations, *J. Geophys. Res.*, 2004, vol. 109, A10209.
https://doi.org/10.1029/2004JA010576

7. Hartinger, M.D., Zou, S., Takahashi, K., et al., Nightside Pi2 wave properties during an extended period with stable plasmapause location and variable geomagnetic activity, *J. Geophys. Res.*, 2017, vol. 122, no. 12, pp. 12006−12018.
https://doi.org/10.1002/2017JA024708

8. Keiling, A. and Takahashi, K., Review of Pi2 models, *Space Sci. Rev.*, 2011, vol. 161, pp. 63−148.

9. Kim, K.-H., Takahashi, K., Lee, D.-H., Sutcliffe, P.R., and Yumoto, K., Pi2 pulsations associated with poleward boundary intensifications during the absence of substorms, *J. Geophys. Res.*, 2005, vol. 110, A01217.
https://doi.org/10.1029/2004JA010780

10. Lee, D.H., On the generation mechanism of Pi2 pulsations in the magnetosphere, *Geophys. Res. Lett.*, 1998, vol. 25, pp. 583−586.

11. Lysak, R.L., Song, Y., Sciffer, M.D., and Waters, C.L., Propagation of Pi2 pulsations in a dipole model of the magnetosphere, *J. Geophys. Res.*, 2015, vol. 120, pp. 355−367.

12. Martines-Bedenko, V.A., Pilipenko, V.A., Engebretson, M.J., and Moldwin, M.B., Time−spatial correspondence between Pi2 wave power and ultra-violet aurora bursts, *Russ. J. Earth Sci.*, 2017, vol. 17, pp. 1−14.
https://doi.org/10.2205/2017ES000606

13. Pilipenko, V. and Heilig, B., ULF waves and transients in the topside ionosphere, *Low-Frequency Waves in Space Plasmas*, 2016, Keiling, A., Lee, D.H., and Nakariakov, V., Eds., Wiley/Am. Geophys. Union, 2016, pp. 15−29.

14. Pilipenko, V., Fedorov, E., Heilig, B., and Engebretson, M.J., Structure of ULF Pc3 waves at low altitudes, *J. Geophys. Res.*, 2008, vol. 113, A11208.
https://doi.org/10.1029/2008JA013243

15. Shinohara, M., Yumoto, K., Yoshikawa, A., et al., Wave characteristics of daytime and nighttime Pi2 pulsations at the equatorial and low latitudes, *Geophys. Res. Lett.*, 1997, vol. 24, pp. 2279−2282.

16. Sutcliffe, P.R. and Luhr, H., A comparison of Pi2 pulsations observed by CHAMP in low earth orbit and on the ground at low latitudes, *Geophys. Res. Lett.*, 2003, vol. 30, 2105.
https://doi.org/10.1029/2003GL018270

17. Takahashi, K., Ohtani, S., and Yumoto, K., AMPTE CCE observations of Pi2 pulsations in the inner magnetosphere, *Geophys. Res. Lett.*, 1992, vol. 19, pp. 1447−1450.

18. Teramoto, M., Nishitani, N., Pilipenko, V., et al., Pi2 pulsation simultaneously observed in the E and F region ionosphere with the *SuperDARN* Hokkaido radar, *J. Geophys. Res.*, 2014, vol. 119, pp. 3444−3462.

19. Waters, C.L., Lysak, R.L., and Sciffer, M.D., On the coupling of fast and shear Alfvén wave modes by the ionospheric hall conductance, *Earth Planets Space*, 2013, vol. 65, pp. 385−396.

20. Yeoman, T.K. and Orr, D., Phase and spectral power of mid-latitude Pi2 pulsations: Evidence for a plasmaspheric cavity resonance, *Planet. Space Sci.*, 1989, vol. 37, pp. 1367−1383.

Translated by N. Topchiev